Supplementary Information

Growth Rate-Dependent Coordination of Catabolism and Anabolism in the Archaeon *Methanococcus maripaludis* under Phosphate Limitation

Wenyu Gu[a]*, Albert L. Müller[a]*, Jörg S. Deutzmann[a], James R. Williamson[b], & Alfred M. Spormann[a,c]

[a] Department of Civil and Environmental Engineering, Stanford University, Stanford, USA

[b] Department of Integrative Structural and Computational Biology, Department of Chemistry, the Skaggs Institute for Chemical Biology, the Scripps Research Institute, La Jolla, USA

[c] Department of Chemical Engineering, Stanford University, Stanford, CA, USA

Correspondence: AM Spormann, Departments of Chemical Engineering, and of Civil and Environmental Engineering, Stanford University, Stanford, USA

Email: spormann@stanford.edu

*** These authors contributed equally to this work.**

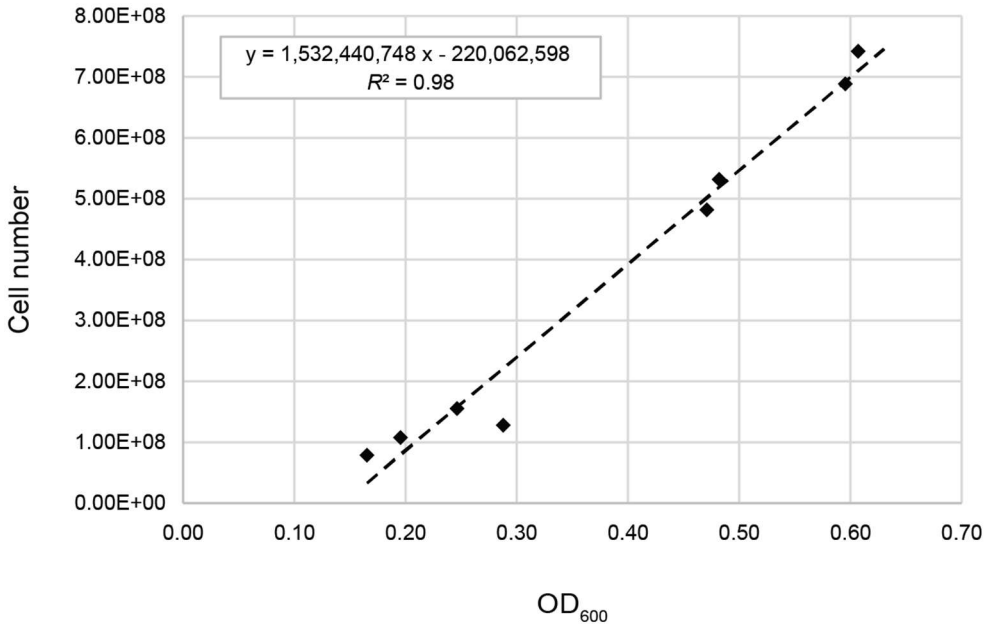

Figure S1. Calibration of cell density versus cell number. OD_{600} measurements correlated linearly to cell number determined by counting ≥1,000 cells using a Petroff-Hausser Counting Chamber and the resulting calibration curve (y = 1,532,440,748 x – 220,062,598, R^2 = 0.98) was used for conversion.

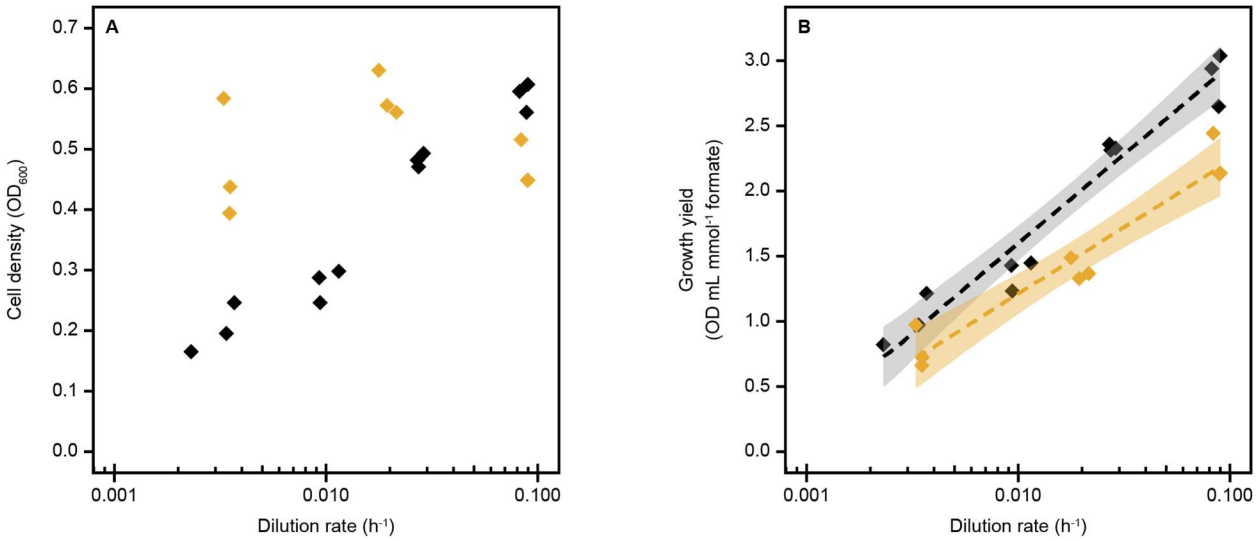

Figure S2. Cell density and growth yield of *M. maripaludis*. (A) OD_{600} values at different growth rates under phosphate-limited (gold, this study) and formate-limited (black, [1]) conditions. Due to decreasing yield at slower growth rates, additional formate in form of formic acid was added to slower growth rates of phosphate-limited cells (total concentrations: 200 mM at fast, 400 mM at intermediate, and 600 mM at

slow growth rates) in order to keep cell densities above the threshold where cells would become formate- instead of phosphate-limited. (B) Apparent molar growth yields of *M. maripaludis* cells on formate correlated logarithmically with dilution rate under both phosphate-limited (gold, y= 0.15ln(x) + 1.11, R^2 = 0.93, $p < 0.01$, this study) and formate-limited (black, y = 0.20ln(x) + 1.47. $R^2 = 0.95$, $p < 0.01$, [1]) conditions. Shaded areas depict 95% confidence intervals.

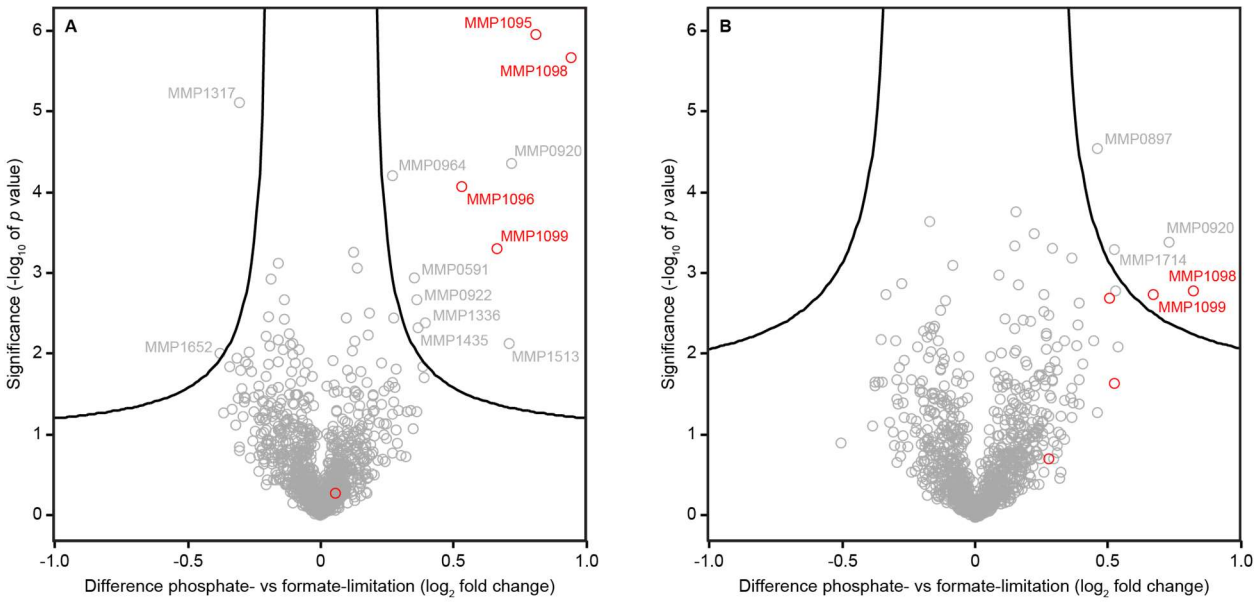

Figure S3. Comparison of protein expression of *M. maripaludis* under formate vs. phosphate limitation at fast growth rates (A) and at very slow growth rates (B). Scatter plots show log2-fold changes and -log10 *p* values from two-sided Student's t-test comparisons. Proteins above the black line are significantly enriched under phosphate- (top right) or formate-limited (top left) conditions using a false discovery rate of 0.05 and S0 of 0.1 as cutoff. Proteins of the phosphate uptake operon *pst* (red circles) are generally upregulated under phosphate-limited conditions. A) Comparison of average mass fraction of samples run at fast (between 0.082 and 0.090 h^{-1}) dilution rates under phosphate limitation (P-F1, P-F2, P-F3) with samples run under formate limitation (F1, F2, F3, [1]). B) Comparison of average mass fraction of samples run at very slow (between 0.002 and 0.004 h^{-1}) dilution rates under phosphate limitation (P-XS1, P-XS2, P-XS3) with samples run under formate limitation (XS1, XS2, XS3 [1]).

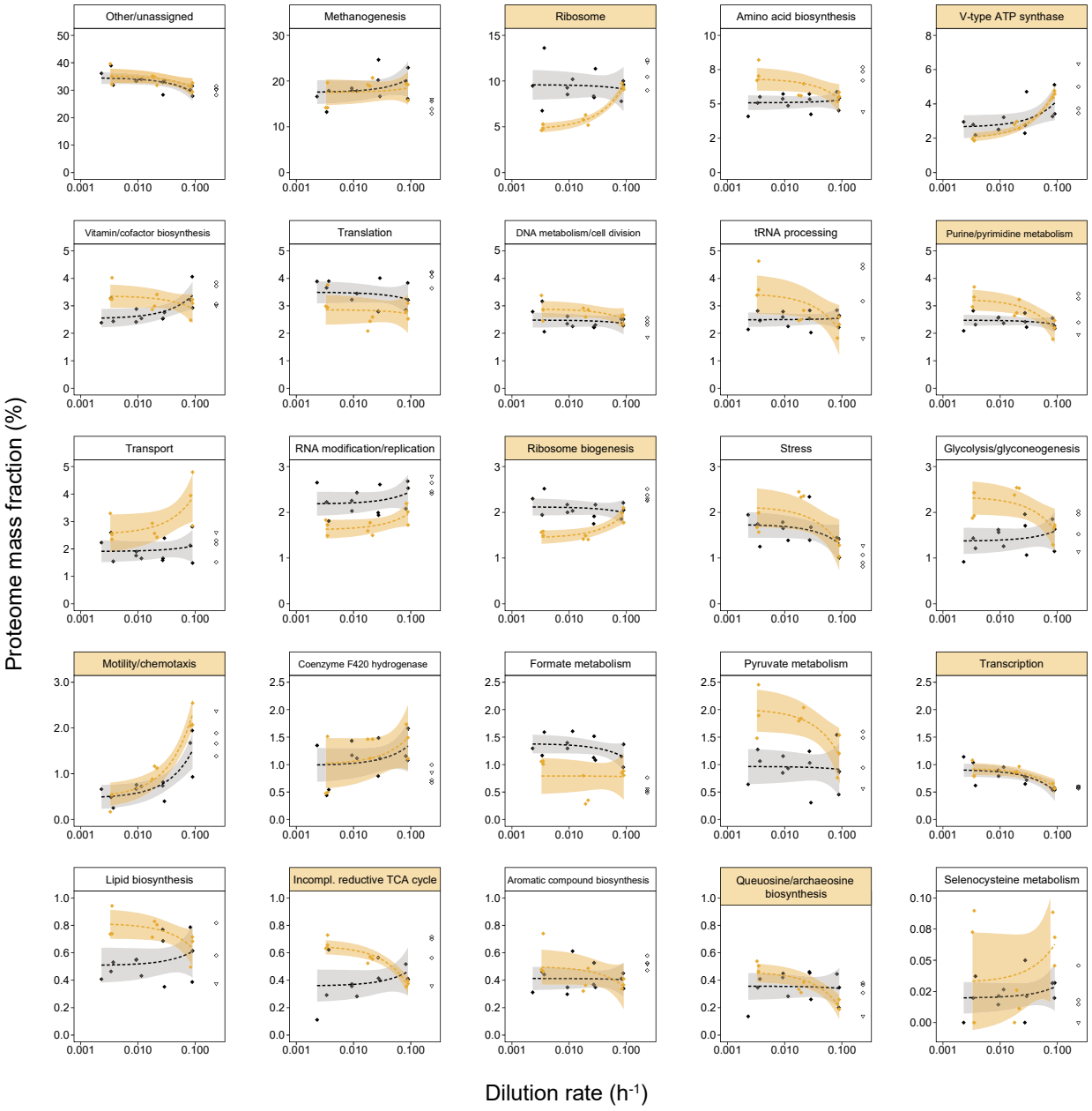

Figure S4. Proteome allocation to functional sub-systems. Mass fraction of total proteome is shown for phosphate-limited growth (gold diamonds, this study) with data under formate limitation shown as a reference (black diamonds, [1]). Sectors with significant growth rate dependence (significantly non-zero slope of linear regression, $p < 0.05$ after correction for multiple comparisons) under phosphate-limited conditions are highlighted in gold. Results from an exponential phase batch culture sample are shown (open symbols), but not used for regression analysis. Shaded areas depict 95% confidence intervals.

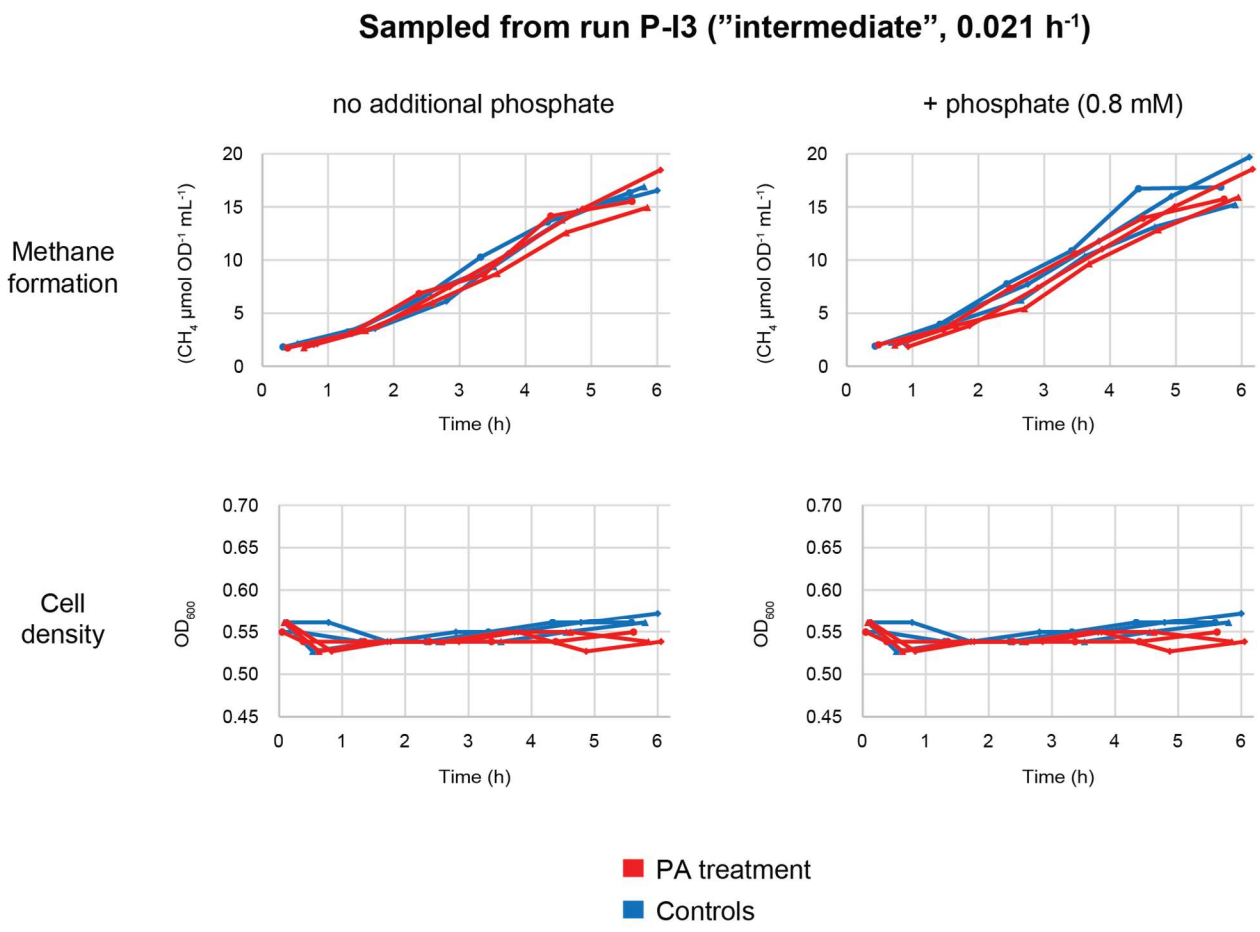

Figure S5. Cells grown in continuous culture were transferred to anoxic Hungate tubes with 150 mM sodium formate, 1 mM sodium sulfide, as well as 0.8 mM K_2HPO_4 and/or 5 µg mL^{-1} translation inhibitor pseudomonic acid (PA) when indicated. Upper panel shows specific methane production rate as the slopes of methane accumulation (per OD_{600}) during the first 6h after formate addition. Lower panel showed cell density (OD_{600}) during the same time frame. The data shows that cells are phosphate limited - phosphate addition allowed cells to grow, but did not influence methane production rate.

Table S1. Individual proteins with significant correlation with growth rate, ordered by slope of the linear regression.

Locus	Annotation (Uniprot)	*Assigned functional subsystem*	Regression		*p* value	Mass fraction	
			Slope	*SE*[1]	(adjusted)	average	*SD*[2]
MMP1403	50S ribosomal protein L22	Ribosome	0.302	*0.044*	0.011	0.08%	*0.03%*
MMP0258	50S ribosomal protein L12	Ribosome	0.239	*0.026*	0.004	0.81%	*0.55%*
MMP1433	50S ribosomal protein L11	Ribosome	0.220	*0.046*	0.048	0.22%	*0.05%*
MMP1045	V-type ATP synthase subunit B	V-type ATP synthase	0.202	*0.028*	0.010	0.79%	*0.19%*
MMP1404	30S ribosomal protein S3	Ribosome	0.176	*0.028*	0.013	0.27%	*0.09%*
MMP1415	50S ribosomal protein L6	Ribosome	0.171	*0.026*	0.011	0.20%	*0.04%*
MMP1325	30S ribosomal protein S9	Ribosome	0.170	*0.037*	0.049	0.06%	*0.02%*
MMP0163	Putative arsenical pump-driving ATPase	Stress	0.166	*0.030*	0.023	0.23%	*0.07%*
MMP0447	Nitrogenase related protein	Other/unassigned	0.161	*0.031*	0.032	0.04%	*0.02%*
MMP1042	V-type ATP synthase subunit C	V-type ATP synthase	0.151	*0.020*	0.008	0.46%	*0.30%*
MMP1412	50S ribosomal protein L5	Ribosome	0.144	*0.012*	0.001	0.15%	*0.02%*
MMP1418	50S ribosomal protein L18	Ribosome	0.134	*0.028*	0.045	0.13%	*0.04%*
MMP1044	V-type ATP synthase subunit A	V-type ATP synthase	0.129	*0.011*	0.001	0.96%	*0.26%*
MMP1640	S-adenosylmethionine synthase	Amino acid biosynthesis	0.129	*0.014*	0.004	0.26%	*0.08%*
MMP1543	50S ribosomal protein L3	Ribosome	0.127	*0.022*	0.021	0.31%	*0.11%*
MMP0975	Molybdate ABC transporter substrate-binding protein	Vitamin/cofactor biosynthesis	0.112	*0.018*	0.014	0.24%	*0.18%*
MMP1046	V-type ATP synthase subunit D	V-type ATP synthase	0.105	*0.021*	0.043	0.17%	*0.05%*
MMP1319	30S ribosomal protein S13	Ribosome	0.092	*0.014*	0.011	0.16%	*0.05%*
MMP1054	Heterodisulfide reductase subunit C2	Methanogenesis	0.088	*0.012*	0.008	0.20%	*0.08%*
MMP0625	50S ribosomal protein L14e	Ribosome	0.077	*0.012*	0.013	0.06%	*0.03%*
MMP1249	Formylmethanofuran dehydrogenase subunit C	Methanogenesis	0.058	*0.012*	0.048	0.27%	*0.10%*
MMP1666	Flagellin	Motility/chemotaxis	0.053	*0.010*	0.038	0.08%	*0.06%*
MMP1671	Flagella accessory protein E	Motility/chemotaxis	0.053	*0.007*	0.008	0.16%	*0.11%*
MMP1563	Tetrahydromethanopterin S-methyltransferase subunit B	Methanogenesis	0.048	*0.010*	0.049	0.20%	*0.13%*
MMP1190	Peptidyl-prolyl cis-trans isomerase	Vitamin/cofactor biosynthesis	0.048	*0.005*	0.004	0.07%	*0.02%*
MMP1670	Flagella accessory protein D	Motility/chemotaxis	0.038	*0.006*	0.012	0.33%	*0.16%*
MMP1667	Flagellin	Motility/chemotaxis	0.015	*0.002*	0.011	0.04%	*0.06%*
MMP0887	Uncharacterized protein	Other/unassigned	-0.124	*0.007*	0.002	0.02%	*0.01%*
MMP1347	Archaeal histone B	Other/unassigned	-0.159	*0.034*	0.049	0.25%	*0.04%*

[1] *Standard error*

[2] *Standard deviation*

Dataset S1 (separate file). Collection of data accompanying chemostat experiments at different growth rates.

Dataset S2 (separate file). Overview of functional classification of *M. maripaludis proteins*, relative mass fraction data of protein abundance determined by spectral counting, and relative quantification against a ^{15}N labeled reference.

References

[1] Müller AL, Gu W, Patsalo V, Deutzmann JS, Williamson JR, Spormann AM. An alternative resource allocation strategy in the chemolithoautotrophic archaeon Methanococcus maripaludis. *Proc Natl Acad Sci U S A* 2021; 118: 1–8.